

Synergistic Effect of Incorporation of BG 45S5 and Silver Nanoparticles on β -TCP Scaffolds: Structural Characterization and Evaluation of Antimicrobial Activity and Biocompatibility

B. R. Spirandeli^a, E. F. Martins^b, L. R. M. Dona^b, R. G. Ribas^b , T. M. B. Campos^b, E. Esposito^a,
G. P. Thim^b, D. B. Tada^a, E. S. Trichês^{a*} 

^aUniversidade Federal de São Paulo (UNIFESP), 12231-280, São José dos Campos, SP, Brasil.

^bInstituto Tecnológico de Aeronáutica (ITA), 12228-900, São José dos Campos, SP, Brasil.

Received: February 14, 2023; Revised: May 13, 2023; Accepted: May 21, 2023

Bacterial infections after implant surgical procedures are a complication observed in many surgeries to treat bone injuries or diseases. Bacteria can attach to the surface of the implant producing biofilms, and if treatment with antibiotics does not work, further surgery is necessary to remove the infected implant. Among the biomaterials for bone implants, bioceramics based on calcium phosphates (CaPs) such as β -TCP stand out, due to their chemical similarity with bone and high bioresorbability. β -TCP has the characteristic of easily accommodating in its crystalline structure reasonable amounts of doping elements, such as monovalent and trivalent ions, which makes it an efficient transporter of drugs, molecules, and therapeutic ions. The objective of this work was the incorporation of bioactive glass (BG 45S5) via sol-gel and silver nanoparticles (Ag-NPs) in β -TCP scaffolds, aiming to confer antimicrobial activity to the scaffolds, without prejudice to biocompatibility. XRD and FT-IR analysis indicated structural changes after the incorporation of BG 45S5 and Ag-NPs in β -TCP scaffolds, and these compounds induced the partial transformation of the β -TCP phase into α -TCP phase and the formation of sodium-calcium silicates and silver silicates. The FT-IR spectra showed characteristic bands of α -TCP after incorporation, in addition to the predominant bands of β -TCP. Biocompatibility after incorporation of BG 45S5 was improved, with a significant increase in cell viability. After the incorporation of Ag-NPs, cell viability was maintained at an acceptable level, no cytotoxic behavior was observed, and the scaffolds showed antibacterial and antifungal activity. The results indicate that BG 45S5 and the Ag-NPs incorporated showed a synergistic behavior, conferring antimicrobial activity to the scaffolds without compromising biocompatibility, showing great potential for applicability in tissue engineering.

Keywords: *Scaffolds, 45S5 bioactive glass, β -TCP, silver nanoparticles, sol-gel, antimicrobial activity, cytotoxicity.*

1. Introduction

Surgical procedures are performed all over the world to repair or replace bone tissue damaged by trauma, injury, or disease. Musculoskeletal diseases, traumas arising from accidents, and arthritis are examples of diseases related to the musculoskeletal system that affect more people, due to the increase in life expectancy and more active profile of the population¹. Although bone tissue can regenerate itself, extensive defects and disease-associated bone loss require the implantation of bone grafts to fill these defects. Currently, the most used treatment system is still based on the use of autografts or allografts, which are natural implants taken from the patient or a compatible donor, respectively. This system has significant limitations, such as reduced availability and high morbidity at the place of collection, in addition to the possibility of disease transmission and the patient's autoimmune response, in the case of allografts. Thus, synthetic grafts have been an alternative to natural

grafts increasingly studied and applied in the treatment of bone lesions.

One of the most common complications after implant surgical procedures is related to bacterial infections in the implant region. According to Yuan et al.², the post-implantation infection rate can reach 43% for previously infected cases. Bacteria can attach to the surface of the biomaterial, forming biofilms and, if antibiotic resistance develops, a new surgery must be performed to remove the implant². Local delivery strategies have been studied to combat infection after implantation, such as loading carbon nanotubes with antimicrobial agents and nanoencapsulating antibiotics^{1,3,4}. However, the slow and controlled release of antibiotics still represents a challenge, and maintaining a bactericidal concentration for a brief period may be insufficient to fight the infection, in addition to increasing the risk of developing antibiotic-resistant bacterial strains^{1,5-7}. In this way, in order to prevent the risk of infection in the long term, a material capable of retaining antimicrobial activity for a longer period is necessary. β -Tricalcium phosphate (β -TCP, β -Ca₃(PO₄)₂)

*e-mail: eliandra.sousa@unifesp.br

has been widely used for manufacturing scaffolds for bone regeneration, due mainly to its great chemical similarity with the mineral phase of bones. β -TCP scaffolds are highly biocompatible and osteoconductive, but their main feature is their high bioresorbability, which allows them to degrade at the end of treatment, releasing non-toxic elements to the body (calcium and phosphorus). The properties of β -TCP can be improved by replacing different ions (monovalent, bivalent, or trivalent) in its structure, such as silver, iron and zinc⁸⁻¹¹. Studies have shown that β -TCP can be used as a highly effective drug and chemical delivery system since the incorporated reagents are homogeneously distributed in the material structure^{2,12}.

The material currently most used to confer antimicrobial activity on β -TCP is silver (Ag)^{2,7,10,12}. Nanometric silver, metallic silver, silver ions, and composites containing silver exhibit antimicrobial activity against various bacterial strains, gram-positive and gram-negative, such as *Staphylococcus aureus* (*S. aureus*) and *Escherichia coli* (*E. coli*), respectively, in addition to fungi and some viruses^{7,13,14}. In addition, Ag can potentiate the action of antibiotics, being able to resensitize resistant bacterial strains, and can be easily added as a dopant to β -TCP^{12,15-18}. According to Vollmer et al.⁷, the antimicrobial action of Ag is related to a multifaceted attack on the structure and cellular functions of microorganisms. Ag has been reported to bind to groups containing oxygen, nitrogen, or sulfur, such as carboxyl groups (-COOH), amino (-NH), and thiol (-SH) of vital intramicrobial structures, leading to enzymatic inactivation and blockage of cytochromatic respiration^{7,10,19-21}. Ag also damages the plasma membrane of the microorganism, increasing its permeability and impairing the regulation of nutrient diffusion across the membrane^{7,22}. Moreover, it is postulated that the interaction with silver can reduce the stability of the DNA helix, inhibiting its replication capacity^{7,20,23,24}. The development of resistance to Ag in microbial strains is significantly hampered due to this multifaceted attack, characteristic of the Ag^{7,20,25}.

Despite the advantages, the use of silver requires care since high concentrations of Ag ions in body fluids can induce cytotoxic effects in some tissues¹⁰. For this reason, Ag nanoparticles (Ag-NPs) used for therapeutic and diagnostic purposes must, invariably, have their cytotoxicity determined^{2,26}. However, silver has shown antimicrobial activity even at low concentrations, while maintaining relatively low cytotoxicity^{10,13,27}. Yuan et al.² studied the antimicrobial activity and cytotoxicity in β -TCP composites doped with 5 and 10 wt% of nanometer Ag. They found that the composites inhibited the proliferation of *S. aureus* and *E. coli* bacteria but were not cytotoxic to human bone marrow mesenchymal stem cells, with no damage to renal or hepatic function *in vivo* tests.

45S5 bioactive glass is also a biomaterial that can be incorporated on porous β -TCP scaffolds to confer antimicrobial activity^{28,29}. It belongs to the SiO_2 - Na_2O - CaO - P_2O_5 system and has properties such as high bioactivity, biocompatibility, and solubility in a physiological environment in addition to the ability to inhibit microbial proliferation³⁰⁻³³. In recent work, it was found that the incorporation of BG 45S5 on β -TCP scaffolds induced an antimicrobial behavior that did not exist in pure β -TCP, preventing the attachment and

growth of *S. aureus* and *E. coli* bacteria, and the fungus *C. albicans*³⁴. Also, it was verified that the antimicrobial activity was accompanied by a significant increase in cell viability, alkaline phosphatase activity, and total protein content. It is known that the rapid dissolution of BG 45S5 in a physiological medium can increase the local pH, induce changes in osmotic pressure and damage the cytoplasmic membrane, which affects intracellular functions essential to the metabolism of the microorganism, such as enzymatic activity³⁵⁻³⁷. Given the reported properties of Ag-NPs and BG 45S5, it is assumed that the joint incorporation of these two components into β -TCP scaffolds has a synergistic effect, resulting in a biomaterial with improved biocompatibility properties and antimicrobial activity.

In this work, β -TCP scaffolds were manufactured by the foam gel casting method, and BG 45S5 was incorporated by means of vacuum impregnation in sol-gel solution, followed by heat treatment at 1200 °C, as described by Spirandeli et al.³⁴ Next, Ag-NPs were incorporated on the β -TCP/45S5 composite scaffolds by means of vacuum impregnation from a colloidal suspension of the nanoparticles, also followed by heat treatment at 1200 °C. The main objective of this work was to study the influence of the incorporation of BG 45S5 and Ag-NPs on the biocompatibility and antimicrobial activity of composite scaffolds obtained by the vacuum impregnation method. In addition to the main objective, the specific objectives of the work were to analyze the influence of the incorporation of these compounds on the crystalline structure and morphology of composite scaffolds.

2. Materials and Methods

2.1. Synthesis and characterization of β -TCP

β -TCP powder was obtained by solid state reaction^{38,39}. Calcium phosphate (CaHPO_4 , Synth, 99.00%) and calcium carbonate (CaCO_3 , Synth, 99.00%) were mixed in a 2:1 molar ratio for 30 minutes. This mixture was then calcined at 1050 °C with a heating rate of 5 °C.min⁻¹ and a residence time of 360 minutes in a muffle furnace (EDG, 3P-S). After synthesis and calcination, the β -TCP powder was ground in a jar mill (Marconi, MA500) for 24 hours with alumina spheres 6 mm in diameter, using a sphere mass:powder ratio of 10:1. After milling, the powder was analyzed by X-ray diffraction (Panalytical Diffractometer, model X'pert Powder) to verify the formation of the crystalline phase (only the presence of the β -TCP phase, JCPDS 00-009-0169 was verified) and by laser diffraction (Cilas, model 1190) to determine the particle size, (average particle size of 1.57 μm and D_{10} = 0.85 μm , D_{50} = 1.46 μm and D_{90} = 2.41 μm).

2.2. Preparation of β -TCP scaffolds

The β -TCP scaffolds were produced by the foam gel casting method. Ceramic suspensions with a solids content of 30% wt were prepared by dispersing the β -TCP powder in an aqueous solution containing organic monomers. The monomers used were N-(hydroxymethyl) acrylamide (HMAM), methacrylamide (MAM), and N,N'-methylenebisacrylamide (MBAM), from Sigma Aldrich, in a 3:3:1 molar ratio (HMAM:MAM:MBAM). The procedure

used to obtain the ceramic foams was described in detail in Spirandeli et al.³⁴ The gelled porous foams were then sintered to obtain the scaffold. Heating was used up to 200 °C at a rate of 5 °C.min⁻¹, from 200 °C to 500 °C with 1 °C.min⁻¹ and 60 minutes of permanence, from 500 °C to 1200 °C with 5 °C.min⁻¹ and 120 minutes of stay³⁴.

2.3. Synthesis of BG 45S5 and Ag-NPs and the incorporation on β -TCP scaffolds

BG 45S5 with a molar composition of 46.1% SiO₂, 26.9% CaO, 24.4% Na₂O, and 2.6% P₂O₅, was produced by the sol-gel method, as previously described by Spirandeli et al.⁴⁰ Briefly, the precursors listed in Table 1 were mixed in a beaker with the silicic acid solution (H₄SiO₄, 0.5 mol.L⁻¹). At the end of the additions and mixing, a clear and transparent sol of 45S5 BG was obtained. This sol was used to incorporate the β -TCP scaffolds and obtain the composite scaffolds of β -TCP/BG, β -TCP/BG/Ag, and β -TCP/BG/Ag_{HT}.

For incorporation of the bioactive glass, the β -TCP scaffolds were immersed in 200 ml of the sol-gel precursor solution of 45S5 BG, inside a vacuum chamber. A pressure of -1 Bar was applied to help the sol fill the interconnected porosity of the scaffolds. After 10 minutes, the scaffolds were removed from the chamber and kept for 10 minutes in an oven at 100 °C. This immersion and drying process was repeated three times in a row. Finally, the scaffolds were dried for 24 hours at 100 °C, to obtain a xerogel inside the pores, and subjected to heat treatment at 1200 °C (heating rate of 5 °C.min⁻¹ and 2 hours at 1200 °C) for melting and incorporating the bioglass. β -TCP scaffolds without bioglass were also subjected to the same treatment, to demonstrate that heat treatment alone does not induce changes in the crystalline phases formed.

The suspension of Ag-NPs was obtained by the Turkevich method, by means of the reduction of silver from a solution of silver nitrate (AgNO₃)^{41,42}. The incorporation of Ag-NPs was performed by the same impregnation and drying process as described above. However, only part of the scaffolds was subjected to heat treatment after impregnation. Six groups of scaffolds were obtained in this study and are detailed in Table 2.

2.4. Characterization of β -TCP scaffolds

The morphology of the scaffolds was analyzed by scanning electron microscopy (SEM) in a TESCAN microscope model MIRA 3 operating at 10 kV. Pore size was measured on SEM images using Image-J software. The geometric porosity of the β -TCP scaffolds was calculated using Equations 1 and 2, where d_T is the β -TCP theoretical density (3.07 g.cm⁻³), $m_{scaffolds}$ is the measured mass (g) and $V_{scaffolds}$ is the calculated scaffold volume (cm³).

$$P(\%) = \left[1 - \left(\frac{d_{Scaffolds}}{d_T} \right) \right] \times 100 \quad (1)$$

$$d_{Scaffolds} = \left(\frac{m_{Scaffolds}}{V_{Scaffolds}} \right) \quad (2)$$

X-ray diffraction analysis (Panalytical Diffractometer, model X'pert Powder) was performed on the powder of

Table 1. Precursors used in the sol-gel synthesis of BG 45S5⁴⁰.

Colloidal Sol-Gel Synthesis		
Intended compound	Precursor	Contents (%mol)
SiO ₂	H ₄ SiO ₄	0,185
P ₂ O ₅	(NH ₄) ₃ PO ₄	0,010
Na ₂ O	NaNO ₃	0,098
CaO	Ca(NO ₃) ₂ ·4H ₂ O	0,110

Table 2. Initial groups of scaffolds used in the work.

Scaffolds groups	Description
β -TCP	Pure β -TCP.
β -TCP/BG	Incorporation BG 45S5 ³⁴ .
β -TCP/Ag	Incorporation Ag-NPs.
β -TCP/Ag _{HT}	Incorporation Ag-NPs and heat treatment at 1200 °C.
β -TCP/BG/Ag	Incorporation BG 45S5 and Ag-NPs.
β -TCP/BG/Ag _{HT}	Incorporation BG 45S5, Ag-NPs, and heat treatment at 1200 °C.

the macerated scaffolds. The analysis was obtained in the range of 20 to 40°, with a scan step of 10.1600 s, step size of 0.0170°, and CuK _{α} radiation. After XRD analyses, the scaffold groups where silver nitrate was found were discontinued.

FT-IR analyses of the macerated scaffolds were performed on a Perkin Elmer Spectrum, Frontier model, covering the wavenumber range from 4000 to 400 cm⁻¹ in UATR mode using a diamond crystal.

2.5. Cell viability assays

The biocompatibility of the scaffolds was evaluated by cell viability assays. Cell viability assays were measured after incubation of mouse embryonic fibroblasts (MEF) with the different groups of scaffolds. Cells were cultured in Dulbecco's Modified Eagle Medium (DMEM), supplemented with 10% fetal bovine serum (FBS). They were incubated for a period of 48 hours in an oven at 37 °C in a humid atmosphere containing 5% CO₂ in cell culture flasks until about 80% confluence. After confluence, cells were washed with phosphate-buffered saline (PBS) and detached with 0.25% trypsin solution. Cell suspensions were centrifuged at 3000 rpm for 5 minutes. Five samples (8 mm in diameter and 2 mm in thickness) from each of the scaffold's groups were sterilized and placed into 48-well plate. Then, they were seeded with 100 μ L of the MEF cells suspension in DMEM 10% FBS at a concentration of 10⁴ cells/well, followed by the addition of 500 μ L of DMEM 10% FBS culture medium. Finally, the plates were incubated for 48 hours at 37 °C and 5% CO₂. Following, the culture medium was removed and 500 μ L of MTT solution (0.5 mg.mL⁻¹) was added to each well. The plate was incubated for 3h. Then, the solution was removed from each well and 500 μ L of DMSO was added to the wells to dissolve the formazan salt that was formed by the viable cells. Then, the solution was removed from the

wells and placed into empty wells to measure the absorbance. The absorbance was measured after 1.5 h at 540 nm in a plate reader (Biotek Plate Reader). Cell viability was calculated by considering the average absorbance of the cells grown in the plate in the absence of samples as 100% of viability. DMSO 20% was used as positive control of cytotoxicity. The data obtained were statistically analyzed using the One-way ANOVA test, considering p-value less than 0.05, and using the GraphPad Prism software.

2.6. Antimicrobial assays

Antimicrobial activity was evaluated using disk diffusion and minimum inhibitory concentration (MIC) assays. The first has the purpose of evaluating the sensitivity of microorganisms to the samples tested, while the second allows quantifying the inhibitory effect of the samples on the microorganisms. In the disk diffusion assays the microorganisms *Candida albicans* ATCC 10231, *Escherichia coli* ATCC 25992, and *Staphylococcus aureus* ATCC 6538 were used at a concentration of approximately 1×10^8 cel.mL⁻¹. These microorganisms were inoculated into Petri dishes (diameter of 90 mm) containing solidified Mueller-Hinton agar (MHA) medium. As positive controls for the bacteria, 5 µg of ciprofloxacin or 30 µg of tetracycline were used and applied in antibiogram discs. The positive fungal controls were discs containing 100 IU of nystatin or 25 µg of fluconazole. Negative controls consisted of plates containing only the inoculated microorganisms, to verify their growth without the influence of any substance. The plates were incubated in a bacteriological oven at 37 °C for 24 h and, after the incubation period, the inhibition halos, when present, were measured with a digital caliper.

Minimum inhibitory concentration (MIC) assays were performed by suspending samples in Mueller-Hinton broth (MHB) medium, using the same microorganisms applied in the disk-diffusion assay and the same cell concentration. The controls for this assay were Tetracycline Hydrochloride (*E. coli* and *S. aureus*) and Amphotericin B (*C. albicans*), at concentrations of 8 µg.mL⁻¹ and 2 µg.mL⁻¹, respectively. As the samples are not soluble in the culture medium, a suspension was prepared from the powder obtained after maceration. For all samples tested, 4 concentrations were used, 100 µg.mL⁻¹, 50 µg.mL⁻¹, 25 µg.mL⁻¹, and 12.5 µg.mL⁻¹, in order to verify the influence of concentration on inhibition. Assays were performed in 15 mL Falcon tubes, containing 10 mL of volume applied to the assay (considering medium, inoculum, antibiotics, and samples). The tubes were incubated in an oven with agitation of 180 RPM and temperature of 37 °C for 24 h. At the end of the incubation period, 200 µL aliquots were read in a microplate reader (Biotek Plate Reader) at 595 nm, in triplicate. Samples of the medium containing the different uninoculated concentrations were also prepared, to rule out the influence of the samples and the culture medium on the absorbance obtained. The inhibition obtained in the assays with the positive controls and samples was calculated by Equation 3, where Abs_{sample} is the average of the absorbance readings of the sample subtracted from its respective value in the uninoculated sample and Abs_{inocuo} is the value obtained from the absorbance referring to 100% growth.

$$Inhibition(\%) = 100 - \left(\left(\frac{Abs_{sample}}{Abs_{inocuo}} \right) * 100 \right) \quad (3)$$

Samples that showed inhibition greater than 60% were considered positive efficacy. The results referring to the disk diffusion assay and MIC were statistically evaluated using the One-way ANOVA test, considering a p-value less than 0.05, and using the GraphPad Prism software (GraphPad Software, La Jolla California USA, www.graphpad.com).

The pH was also monitored in the two antimicrobial tests. In the disk-diffusion test, six measurements were performed in the inhibition halos formed around the samples, as well as in points of the microorganism growth area in the Petri dish. The Agar and the broth medium used in the disk diffusion and MIC tests were prepared with a pH = 7. In the MIC tests, three measurements were performed on the suspensions of the scaffold groups, on the pure medium, and on the negative controls of the microorganisms.

3. Results and Discussion

The scaffolds showed an average porosity, measured by the geometric method, of $81.5 \pm 1.5\%$. Figure 1 shows the diffractograms of β-TCP, β-TCP/BG, β-TCP/Ag, β-TCP/Ag_{HT}, β-TCP/BG/Ag and β-TCP/BG/Ag_{HT} scaffolds. The β-TCP scaffolds showed only the β-TCP phase (β-Ca₃(PO₄)₂, JCPDS 00-009-0169). There was no difference between the diffractograms of the β-TCP and β-TCP/Ag scaffolds. The diffractogram of the β-TCP/BG scaffolds showed, besides β-TCP crystalline phase, several new peaks attributed to the α-TCP phases (α-Ca₃(PO₄)₂, JCPDS 00-009-0348), high-combeite (Na_{15.78}Ca₃(Si₆O₁₂), JCPDS 01-078-1650) and wollastonite (CaSiO₃, JCPDS 00-027-0088). The formation of these phases in β-TCP/BG scaffolds was discussed in recent work³⁴. The transformation of the β-TCP phase into α-TCP is attributed to the action of the existing silicon in the composition of the incorporated bioactive glass, which stabilizes the α-TCP phase at lower temperatures during heat

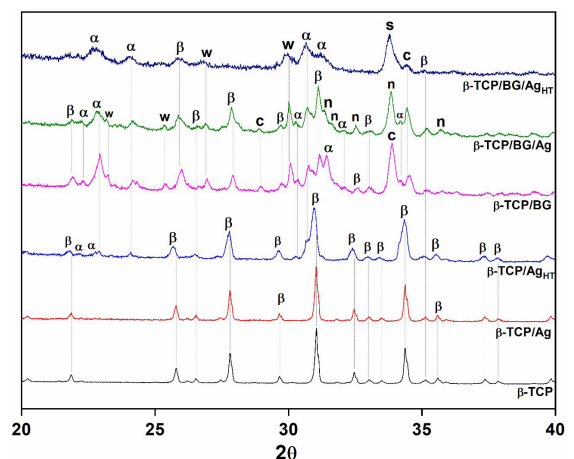


Figure 1. XRD patterns of β-TCP scaffolds prepared via gel casting and incorporation of BG 45S5 and Ag-NPs. β: β-Ca₃(PO₄)₂; α: α-Ca₃(PO₄)₂; c: Na_{15.78}Ca₃(Si₆O₁₂); w: CaSiO₃; n: Ag₃(SiO₄)₂NO₃; S: Ag₄SiO₄.

treatment⁴³⁻⁴⁵. The observed calcium and sodium-calcium silicates, wollastonite and high-combeite, are characteristic phases of the crystallization of 45S5 BG, and also common in β -TCP/BG 45S5 composites⁴⁶⁻⁵⁰. The formation of α -TCP improves bioactivity, dissolution rate, and the ability to replace scaffolds with new bone while silicates have good mechanical strength and bioactivity^{48,51,52,53}.

In the diffractogram of the β -TCP/Ag_{HT} scaffold, besides the majority β -TCP phase, peaks of the α -TCP phase were observed. This suggests that impregnation with the Ag-NPs suspension followed by heat treatment at 1200 °C had a similar effect to that one observed with 45S5 bioglass, stabilizing the α -TCP phase at temperatures lower than the theoretical ones³⁴. Additionally, it was found that several β -TCP peaks appeared slightly shifted from the standard (JCPDS 00-009-0169), a shift that reached 0.9° for some peaks. This displacement of the peaks due to the incorporation of silver has been previously reported in the literature. Hoover et al.¹² verified a shift in β -TCP peaks in composites containing 1% and 2% wt. Ag₂O, and reported an increase in the α -TCP phase formed as the increase of Ag in the β -TCP matrix. The absence of Ag⁺ or Ag₂O peaks and the partial transformation of the β -TCP phase into α -TCP may indicate the incorporation of Ag-NPs in the β -TCP structure after heat treatment at 1200 °C.

The incorporation of Ag in the structure of β -TCP occurs by a different mechanism than that observed with silicon (Si) in the glass. While Si enters the lattice through substitution at tetrahedral sites of PO₄²⁻ by SiO₄⁴⁻, it has been reported that Ag preferentially occupies vacant Ca²⁺ (4) sites in the β -TCP unit cell⁹. Yoshida et al.⁸ demonstrated that the crystal structure of β -TCP can accommodate approximately 9 mol% of monovalent ions, and developed a mechanism that describes this occupation: $2M^+ = Ca^{2+} + V_{Ca(4)}$, where M⁺ is the monovalent metal ion and V_{Ca(4)} a Ca²⁺(4) vacancy. Singh et al.⁹ demonstrated, through the analysis of the

occupancy factors refined by the Rietveld method, the preferential occupancy of Ag⁺ in the Ca²⁺(4) sites of β -TCP, and that the charge compensation occurs by the mechanism proposed by Yoshida et al.⁸ for monovalent ions.

The diffractograms of the β -TCP/BG/Ag and β -TCP/BG scaffolds are quite similar, except for the presence of peaks in the Ag₂(SiO₃)₂NO₃ phase (JCPDS 01-078-1250). The presence of this phase indicates a probable trace of silver nitrate (AgNO₃) in the impregnation suspension. Thus, the β -TCP/BG/Ag and β -TCP/Ag scaffolds were discontinued, and the study continued only with those submitted to heat treatment after impregnation with the nanoparticles, due to the high cytotoxicity of AgNO₃. No AgNO₃ was observed in the scaffold of β -TCP/Ag_{HT} and β -TCP/BG/Ag_{HT}, since all nitrate is eliminated during the heat treatment at 1200 °C.

The diffractogram of the β -TCP/BG/Ag_{HT} scaffold (impregnated with 45S5 BG and Ag-NPs and exposed to heat treatment at 1200 °C) showed significant changes compared to the others. The transformation of the β -phase into α -TCP was greater, leaving few peaks of the β -TCP phase in the diffractogram. Calcium and sodium-calcium silicates were maintained, and the formation of silver silicate Ag₂SiO₄ (JCPDS 00-012-0741) was observed as the main peak, indicating that the incorporated bioglass may have acted to anchor the nanoparticles impregnated silver.

Figure 2 shows the SEM images of the scaffold surfaces. Figures 2a, e, b, f, c, g, and d, h show the scaffold surfaces of β -TCP, β -TCP/BG, β -TCP/Ag_{HT}, and β -TCP/BG/Ag_{HT}, respectively, with different magnifications. For all scaffolds, the pore size varied between 380 μ m and 180 μ m (average size of 232 \pm 40 μ m), and small pores of 1 μ m were observed in the struts. The macroporosity was interconnected, observing several openings with diameters between 16 and 155 μ m in the pores. The observed morphology is characteristic of cellular ceramics obtained by the foam gel casting method, which gives rise to a macrostructure consisting of spherical

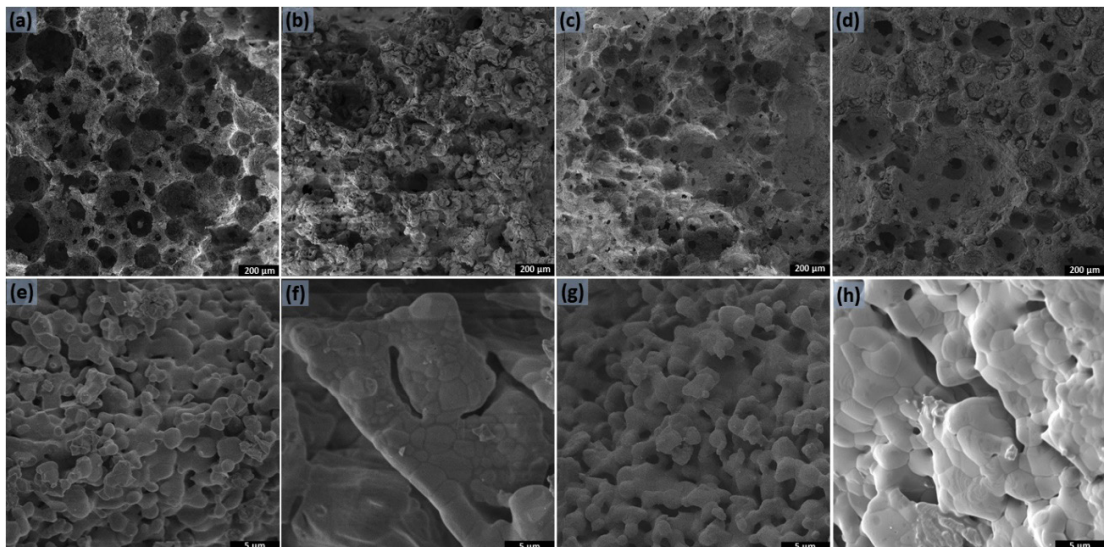


Figure 2. Scanning electron microscopy images of groups of scaffolds under magnification of 200x e 10000x. (a, e) β -TCP; (b, f) β -TCP/BG; (c, g): β -TCP/Ag_{HT}; (d, h) β -TCP/BG/Ag_{HT}.

cells interconnected by circular openings⁵⁴. These openings are formed due to the partial collapse of the liquid film around the gas bubble during the foam formation and gelation process⁵⁵.

SEM images of the β -TCP/BG scaffolds indicated the presence of crystallized combeite plaques on and between the struts. These plaques originate from impregnated BG 45S5 after heat treatment at 1200 °C and were also observed in β -TCP/BG/Ag_{HT} scaffolds, although in smaller amounts. This reduction may be associated with the second heat treatment after impregnation with the Ag-NPs, which melts the combeite formed in the first heat treatment (bioglass incorporation), diluting the plates in the microporous structure of the strut. These results corroborate the XRD diffractograms, which indicated a lower formation of combeite in the β -TCP/BG/Ag_{HT} scaffolds. On the other hand, the β -TCP/Ag_{HT} scaffolds showed no significant change in their structure when compared to the β -TCP scaffolds.

Figure 3 shows the FT-IR spectra of the β -TCP, β -TCP/BG, β -TCP/Ag_{HT} and β -TCP/BG/Ag_{HT} scaffolds. The β -TCP scaffold spectrum showed binding bands characteristic of tricalcium phosphate^{56,57}. Asymmetric elongation binding bands $\nu_3 - (PO_4^{3-})$ between 1020 and 1119 cm⁻¹, asymmetrical elongation bond $\nu_4 - (PO_4^{3-})$ at 604, 590 and 550 cm⁻¹, symmetrical elongation bond $\nu_1 - (PO_4^{3-})$ at 945 and 970 cm⁻¹ were identified. In the β -TCP/BG scaffolds, it was observed that the ν_1 bands showed a significant reduction in intensity, still appearing slightly shifted to the left, and a new ν_3 band appeared at approximately 1000 cm⁻¹. These changes are related to the partial transformation observed in the β -TCP/BG scaffolds, from the β -TCP to α -TCP phase⁵¹.

The β -TCP/Ag_{HT} spectrum showed the typical β -TCP bands, and no evidence of the presence of silver, possibly due to the small amount of nanoparticles that was incorporated into the scaffold. In the β -TCP/BG/Ag_{HT} scaffold, the complete disappearance of the ν_1 bands and part of the ν_3 and ν_4 bands was verified. Table 3 summarizes the binding bands found in the FT-IR spectra of the scaffolds.

Figure 4 shows the results of cell viability assays performed with the scaffolds. The statistical analysis performed using the Tukey test and considering a pValue < 0.05 indicates that, except for the cells incubated with β -TCP/Ag_{HT}, the cell incubation with all scaffolds presented statistically superior cell viability compared to the control (pValue < 0.05). The viability of MEF cells incubated with β -TCP, β -TCP/BG/Ag_{HT} and β -TCP/BG were 14%, 11%, and 40% higher compared to the control, respectively. The cell viability of β -TCP/Ag_{HT} was comparable to the control but slightly lower than that of β -TCP and other scaffolds.

These results indicate that none of the scaffolds were cytotoxic since the limit value for considering a material as

Table 3. Assignment of the binding bands of the FT-IR spectra of the scaffolds.

Bond	Transmittance (cm ⁻¹)	Reference
$\nu_1 - (PO_4^{3-})$	970 e 944	51,56
$\nu_3 - (PO_4^{3-})$	1120, 1080, 1040, 1030, 1020, 1010, 995 e 980	51,56,58
$\nu_4 - (PO_4^{3-})$	605, 590, 550 e 543	51,57

cytotoxic is 70% of viability of cells grown in its presence. The presence of BG 45S5 promoted the cell growth since the viability of MEF cells incubated with this group of scaffolds was higher than the viability of MEF cells incubated with β -TCP. The presence of Ag-NPs led to a slight decrease of cell viability, but it did not compromise the scaffold biocompatibility since the viability of cells incubated with the scaffolds containing Ag-NPs was like the viability of cells grown in the control.

The suitable cell compatibility of β -TCP is often reported as it is known to be a bioceramic with high biocompatibility and commonly used as a bone implant material. The higher values of cell viability observed for the cells incubated with β -TCP scaffolds after incorporation of BG 45S5 via sol-gel had already been observed in our previous work³⁴. This behavior was attributed to the presence of Si present in the incorporated bioglass, which during dissolution in the medium of culture is released in the form of SiO_4^{4-} , which can diffuse into the cell and act favorably on intracellular processes

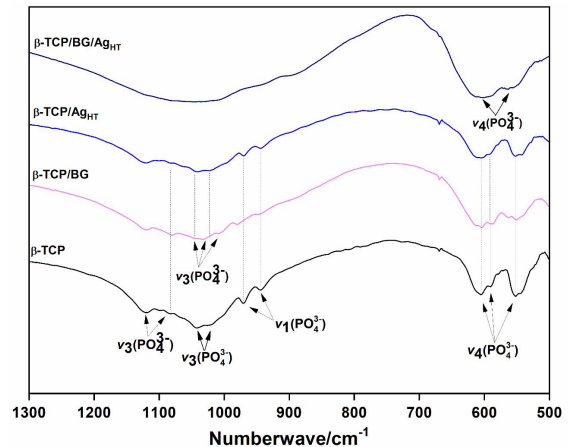


Figure 3. FT-IR spectra of scaffolds.

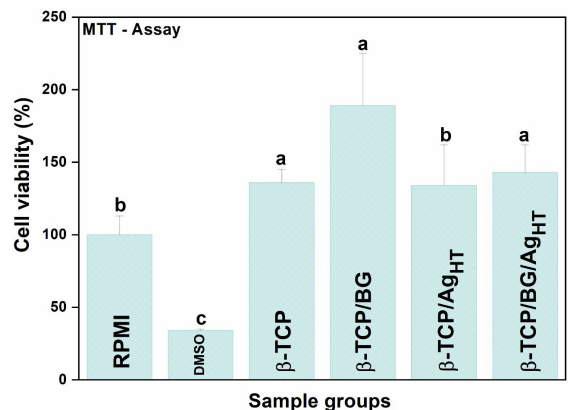


Figure 4. Cell viability of fibroblasts cells measured by MTT assay after 48 h of cell incubation with scaffolds. The indices on the error bar indicate statistical differences between the samples analyzed, with a > b > c. A pair a-a denotes absence of statistical differences, while pair a-b, a-c or b-c indicates that the groups compared were statistically different.

that influence the process of bone formation and collagen biosynthesis^{59,62}. Additionally, since the cell viability was not compromised after incubation with scaffolds containing Ag-NPs, it is expected that this material can be used to provide antimicrobial properties to β -TCP and β -TCP/BG scaffolds.

Figure 5 shows the negative and positive controls of the disk diffusion test for the three microorganisms evaluated: *C. albicans*, *E. coli* and *S. aureus*. Negative controls (Figures 5a, 5d and 5g) indicate that the microorganisms have fixed and proliferated properly on the surface of the culture medium covering the entire plate, which attests to the viability of the inoculum. The positive controls of the three microorganisms (Figures 5b, c, e, f, h, i) showed halos of inhibition of microbial growth. Halos were verified for fluconazole and nystatin controls (Figures 5b and 5c), respectively) used with the fungus *C. albicans*, and for ciprofloxacin and tetracycline controls, used with *E. coli* (Figures 5e and 5f) and with *S. aureus* (Figures 5h and 5i), respectively.

Figure 6 presents photographs of Petri dishes with the scaffolds evaluated for the three microorganisms.

The β -TCP scaffolds showed no inhibition against any of the microorganisms tested, as evidenced by the absence of an inhibition halo in Figures 6a, 6b and 6c), which is in agreement with what has been reported in the literature³⁴. On the other hand, β -TCP/BG scaffolds (Figures 6d, 6e, and 6f) showed inhibition halos for *C. albicans* (Figure 6d) and *S. aureus*.

(Figure 6f), but not for *E. coli* (Figure 6e). The inhibitory behavior of β -TCP/BG was reported in recent work and credited to the increase in the pH of the culture medium by the ionic release of 45S5 BG incorporated into the β -TCP matrix³⁴. This alkalization of the medium can inhibit the growth of microorganisms that commonly live in pH close to neutral or acid, such as *C. albicans* and *S. aureus*, but it was less efficient for *E. coli*, which adapts easily to alkaline media^{63,64}. The β -TCP/Ag_{HT} scaffolds showed inhibition against the three microorganisms (Figures 6g, 6h) and 6i), but it was reduced in the test against *C. albicans* (Figure 6g). Conversely, the β -TCP/BG/Ag_{HT} scaffolds showed potent antimicrobial activity against all tested microorganisms, with inhibition halos of considerable diameters being observed (Figures 6j, 6l, 6m). Figures 7a, 7b and 7c) show the measurements of the diameters of the inhibition halos observed in the photographs of Figure 6.

The three groups of composite scaffolds (β -TCP/BG, β -TCP/Ag_{HT} and β -TCP/BG/Ag_{HT}) showed antibacterial and antifungal activity, except for β -TCP/BG in the test against *E. coli*. For the β -TCP/BG and β -TCP/Ag_{HT} scaffolds, this activity is close to half that of the antibiotics and antifungals used as control groups in the tests against *C. albicans* and *S. aureus*. For β -TCP/Ag_{HT} evaluated against *E. coli*, the diameter of the inhibition halo approximates that of positive controls. The best performance against the three microorganisms was observed for β -TCP/BG/Ag_{HT}. This

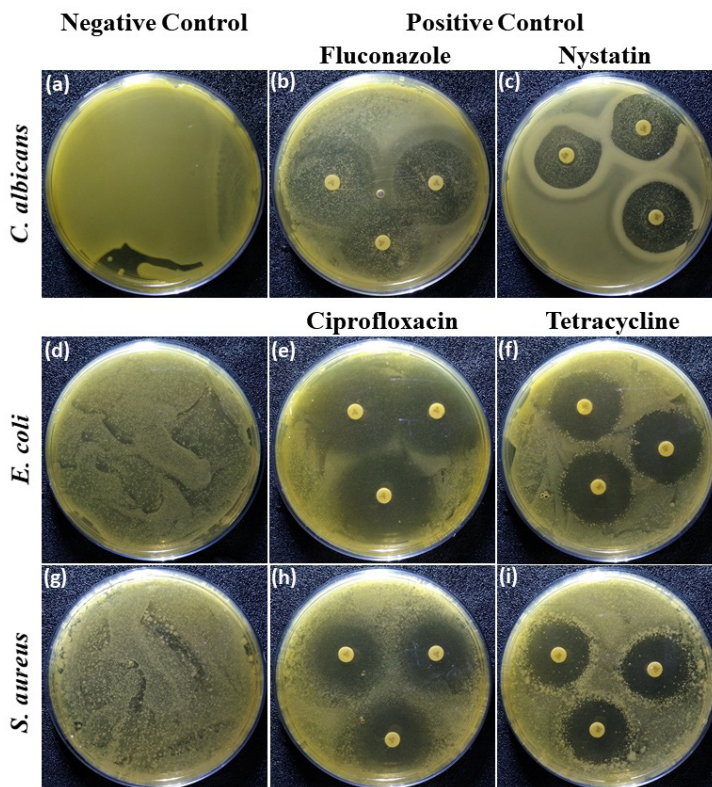


Figure 5. Photographs of Petri dishes with the disk diffusion assay controls: (a), (d) and (g) negative controls in the tests with *C. albicans*, *E. coli* and *S. aureus*; (b) and (c) positive controls of fluconazole and nystatin in the tests with *C. albicans*; (e) and (f) positive controls for ciprofloxacin and tetracycline in the *E. coli* tests; (h) and (i) positive controls of ciprofloxacin and tetracycline in the tests with *S. aureus*.

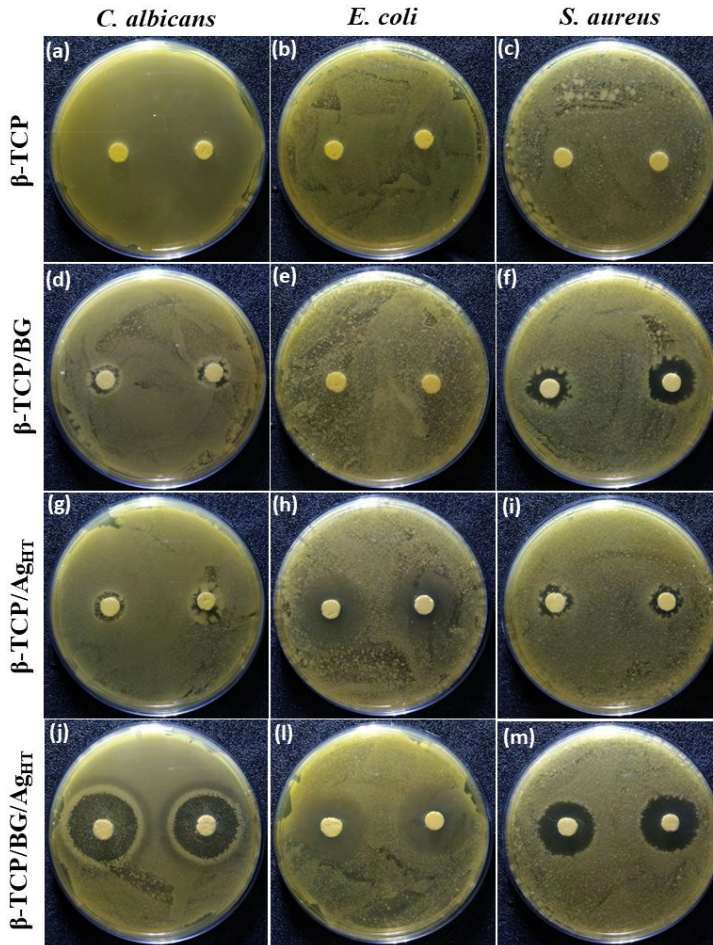


Figure 6. Photographs of Petri dishes from the disk diffusion assay for the β -TCP scaffolds: (a) *C. albicans*, (b) *E. coli*, (c) *S. aureus*; β -TCP/BG: (d) *C. albicans*, (e) *E. coli*, (f) *S. aureus*; β -TCP/Ag_{HT}: (g) *C. albicans*, (h) *E. coli*, (i) *S. aureus*; β -TCP/BG/Ag_{HT}: (j) *C. albicans*, (l) *E. coli*, (m) *S. aureus*.

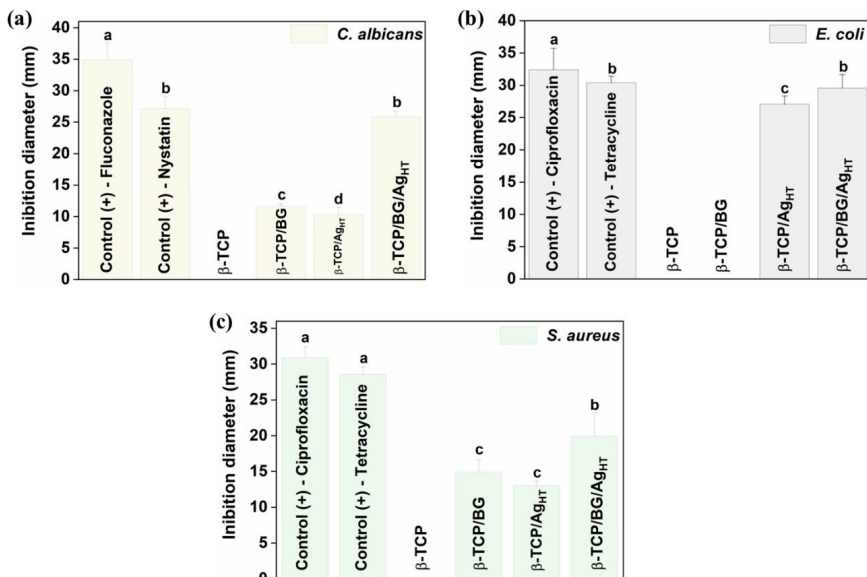


Figure 7. Diameters of the inhibition halos formed in the disk-diffusion tests.

group was statistically like the nystatin control in the test against *C. albicans*, and to the tetracycline control in the test against *E. coli*, considering a pValue < 0.005. It was also statistically superior to β -TCP/BG and β -TCP/Ag_{HT} scaffolds in all tests. This behavior may be associated with cumulative inhibitory effects due to the simultaneous presence of BG 45S5 and Ag-NPs incorporated on the β -TCP scaffold. While the mechanism of antimicrobial activity of bioglass has been related to changes in the pH of the medium, the silver has been acting through a multifaceted attack that ranges from damage to the plasma membrane of the microorganism and enzymatic inactivation to blockage of cytochromatic respiration^{7,20,25}.

Figure 8 presents the results of the minimum inhibitory concentration assay for the scaffolds. In the assays, it was verified that β -TCP did not present significant inhibition at any of the concentrations evaluated and against any of the microorganisms, the same occurring with β -TCP/BG in the assay against *E. coli*, corroborating the disk-diffusion tests. On the other hand, β -TCP/BG showed an inhibition above 60% against *C. albicans* and *S. aureus* at a concentration of 100 mg.mL⁻¹. However, the β -TCP/Ag_{HT} and β -TCP/BG/Ag_{HT} scaffolds showed inhibition above 60% for all microorganisms at a concentration of 100 mg.mL⁻¹. Against *E. coli*, these groups reached an inhibition greater than 60% also at concentrations of 50 and 25 mg.mL⁻¹.

Figure 9 shows the pH results of the disk diffusion and MIC tests. The variations in pH values for the scaffolds were similar in both tests. In the disk-diffusion test, measurements were performed around the samples and in the microbial growth region of the plate, while in the MIC they were performed in the pure medium, negative control and scaffold suspensions. In disk diffusion tests, both *C. albicans* (Figure 9a) and *S. aureus* (Figure 9e) induced a reduction

in the pH of the medium (pH_{Agar} = 7), which indicates that the microorganisms acidified the medium during its growth. *E. coli* (Figure 9c) did not show any statistically significant effect on the pH of the culture medium. There was no statistical difference between the measured pH of the β -TCP scaffolds and the microorganism growth areas (Figures 9a, 9c and 9e). In contrast, β -TCP/BG scaffolds induced a significant increase in the pH of the medium for all microorganisms evaluated (Figures 9a, 9c and 9e). The pH was statistically higher than that measured in the β -TCP scaffolds, in the growth areas and in the agar. The β -TCP/Ag_{HT} scaffolds also showed a statistically higher pH in relation to the β -TCP and the growth area in the tests against *C. albicans* and *S. aureus* (Figures 9a and 9e), and similar to the medium, but not against *E. coli* (Figure 9c). The β -TCP/BG/Ag_{HT} scaffolds showed a pH increase statistically close to that of β -TCP/BG in the tests against *C. albicans* and *S. aureus* and superior in the test against *E. coli* (Figure 9c).

In the MIC test, acidification of the medium was observed with *C. albicans* and *S. aureus* (Figures 9b and 9f), both induced a reduction in the pH of the pure culture medium when compared to the negative control values. *E. coli* evaluation did not show any statistically significant effect on the pH of the culture medium (Figure 9d). The β -TCP/Ag_{HT} scaffolds showed an increase in pH for *C. albicans* and *S. aureus* compared to the negative control (Figures 9b and 9f). This increase may be associated with the absence of growth of microorganisms since the pH measurement was close to that of the pure medium. In the test against *E. coli*, the pH was statistically equal to that of the negative control (Figure 9d). The β -TCP/Ag_{HT} scaffolds showed antimicrobial activity against all microorganisms evaluated, but their activity does not seem to be related to changes in the pH of the medium,

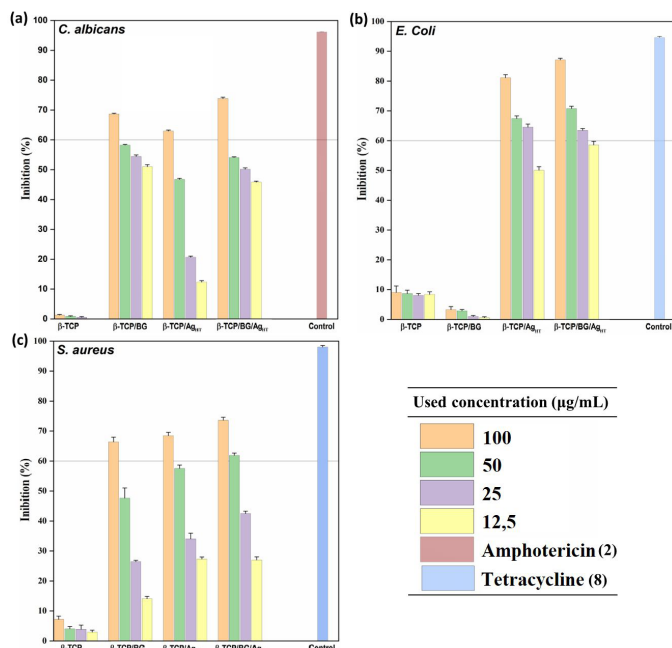


Figure 8. Minimum inhibitory concentration assay. (a) *C. albicans*; (b) *E. coli*; (c) *S. aureus*.

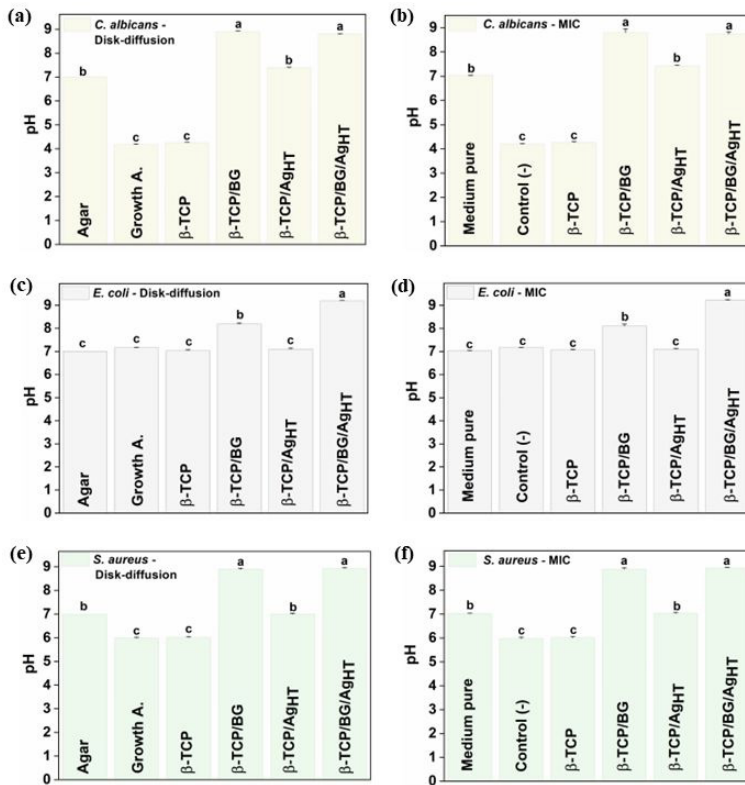


Figure 9. pH values from disk diffusion and MIC tests.

and only the antimicrobial characteristic of silver can be considered. The β -TCP/BG and β -TCP/BG/Ag_{HT} scaffolds presented, in all cases, the highest pH values in relation to the pure medium and the negative control (Figures 9b and 9f). The increase in pH seems to be the main mechanism of inhibition of β -TCP/BG scaffolds against *C. albicans* and *S. aureus*. In tests against *E. coli*, the β -TCP/BG sample did not inhibit the growth of the microorganism, since it is adapted for growth in alkaline medium. In the β -TCP/BG/Ag_{HT} scaffolds there was a cumulative and synergistic inhibitory effect arising from the simultaneous presence of BG 45S5 and Ag-NPs in the scaffold structure. Of the scaffolds studied, the β -TCP/BG/Ag_{HT} scaffold is believed to be most promising for bone tissue recovery and regeneration, as well as for the treatment of bone infections.

5. Conclusion

Bioresorbable, bioactive, and antimicrobial β -TCP scaffolds, incorporated with bioglass and silver nanoparticles, were produced by gel casting followed by a vacuum impregnation method and heat treatment at 1200 °C. Both the incorporation of BG 45S5 and Ag-NPs led to significant changes in the composition, morphology, crystal structure, cell viability, and antimicrobial activity of the β -TCP scaffolds. The partial transformation of β -TCP into α -TCP, the formation of phases of calcium and sodium-calcium silicates of high bioactivity and of silver silicate indicate the ability of the bioglass to anchor the incorporated silver. The dissolution of the ionic species of the incorporated bioglass produces an increase in

the pH of the medium, which contributed to the inhibition of the microorganisms *C. albicans*, *S. aureus* and *E. coli* in the disk diffusion tests. The addition of silver contributed significantly to enhance the antimicrobial activity of the β -TCP/BG scaffolds, as indicated by the disk diffusion and MIC assays. The β -TCP/BG/Ag_{HT} scaffold stood out for presenting improved antimicrobial properties and maintaining suitable cell compatibility. This biomaterial can be considered a potential candidate for application as a synthetic bone implant, providing inhibition of microbial attack and contributing to minimizing the incidence of postoperative infections.

6. Acknowledgements

The authors are grateful to Coordenação de Aperfeiçoamento de Pessoal de Nível Superior – Brasil (CAPES) – Finance Code 001 for the scholarships granted to Ribas R.G. Martins, E.F. and Dona, L. R. M, and São Paulo Research Foundation (FAPESP) for financial support (Proc. 2019/19594-4). Also, the authors would like to thank the NAPCEM Multi-User Laboratory (UNIFESP) and the Plasma and Process Laboratory of the Technological Institute of Aeronautics for the facilities.

7. References

- Hoover S, Tarafder S, Bandyopadhyay A, Bose S. Silver doped resorbable tricalcium phosphate scaffolds for bone graft applications. *Mater Sci Eng C*. 2017;79:763-9.

2. Yuan J, Wang B, Han C, Huang X, Xiao H, Lu X, et al. Nanosized-Ag-doped porous β -tricalcium phosphate for biological applications. *Mater Sci Eng C*. 2020;114:111037.
3. Bose S, Tarafder S. Calcium phosphate ceramic systems in growth factor and drug delivery for bone tissue engineering: a review. *Acta Biomater*. 2012;8:1401-21.
4. King WJ, Krebsbach PH. Growth factor delivery: how surface interactions modulate release in vitro and in vivo. *Adv Drug Deliv Rev*. 2012;64:1239-56.
5. Liu S, Fan C, Jin F, Zhao L, Dai K, Lu J. Preparation and antibacterial activities of porous silver-doped β -tricalcium phosphate bioceramics. *Int J Appl Ceram Technol*. 2015;12:294-99.
6. Porter JR, Ruckh TT, Popat KC. Bone tissue engineering: a review in bone biomimetics and drug delivery strategies. *Biotechnol Prog*. 2009;25(6):1539-60. <https://doi.org/10.1002/btpr.246>.
7. Vollmer NL, Spear JR, Ayers RA. Antimicrobial activity and biologic potential of silver-substituted calcium phosphate constructs produced with self-propagating high-temperature synthesis. *J Mater Sci Mater Med*. 2016;27:104.
8. Yoshida K, Hyuga H, Kondo N, Kita H, Sasaki M, Mitamura M, Hashimoto K, Toda Y. Substitution model of Monovalent (Li, Na, and K), Divalent (Mg), and Trivalent (Al) Metal Ions for beta-Tricalcium Phosphate. *J American Ceram Soc*. 2006;89:688-90.
9. Singh RK, Awasthi S, Dhayalan A, Ferreira JMF, Kannan S. Deposition, structure, physical and in vitro characteristics of Ag-doped β -Ca₃(PO₄)₂/chitosan hybrid composite coatings on Titanium metal. *Mater Sci Eng C*. 2016;62:692-701.
10. Gokcekaya O, Ueda K, Ogasawara K, Kanetaka H, Narushima T. In vitro evaluation of Ag-containing calcium phosphates: effectiveness of Ag-incorporated β -tricalcium phosphate. *Mater Sci Eng C*. 2017;75:926-33.
11. Sinusaite L, Popov A, Antuzevics A, Mazeika K, Baltrunas D, Yang JC, et al. Fe and Zn co-substituted beta-tricalcium phosphate (β -TCP): Synthesis, structural, magnetic, mechanical and biological properties. *Mater Sci Eng C*. 2020;112:110918.
12. Hoover S, Tarafder S, Bandyopadhyay A, Bose S. Silver doped resorbable tricalcium phosphate scaffolds for bone graft applications. *Mater Sci Eng C*. 2017;79:763-9.
13. Ewald A, Hösel D, Patel S, Grover LM, Barralet JE, Gburec U. Silver-doped calcium phosphate cements with antimicrobial activity. *Acta Biomater*. 2011;7:4064-70.
14. Hwang K-S, Hwangbo S, Kim J-T. Silver-doped calcium phosphate nanoparticles prepared by electrostatic spraying. *J Nanopart Res*. 2008;10:1337-41.
15. Morones-Ramirez JR, Winkler JA, Spina CS, Collins JJ. Silver enhances antibiotic activity against gram-negative bacteria. *Sci Transl Med*. 2013;5(190):190ra81.
16. Roy M, Bandyopadhyay A, Bose S. In vitro antimicrobial and biological properties of laser assisted tricalcium phosphate coating on titanium for load bearing implant. *Mater Sci Eng C*. 2009;29:1965-8.
17. Range S, Hagemeyer D, Rotan O, Sokolova V, Verheyen J, Siebers B, et al. A continuous method to prepare poorly crystalline silver-doped calcium phosphate ceramics with antibacterial properties. *RSC Advances*. 2015;5:43172-7.
18. Nayak VV, Tovar N, Hacquebord JH, Duarte S, Panariello BHD, Tonon C, et al. Physicochemical and bactericidal activity evaluation: Silver-augmented 3D-printed scaffolds—An in vitro study. *J Biomed Mater Res B Appl Biomater*. 2022;110:195-209.
19. Kim TN, Feng QL, Kim JO, Wu J, Wang H, Chen GC, et al. Antimicrobial effects of metal ions (Ag 1, Cu 2 1, Zn 2 1) in hydroxyapatite. *J Mater Sci Mater Med*. 1998;9:129-34.
20. Chen W, Oh S, Ong AP, Oh N, Liu Y, Courtney HS, et al. Antibacterial and osteogenic properties of silver-containing hydroxyapatite coatings produced using a sol gel process. *J Biomed Mater Res A*. 2007;82A:899-906.
21. Schierholz J. Efficacy of silver-coated medical devices. *J Hosp Infect*. 1998;40:257-62.
22. Sondi I, Salopek-Sondi B. Silver nanoparticles as antimicrobial agent: a case study on *E. coli* as a model for Gram-negative bacteria. *J Colloid Interface Sci*. 2004;275:177-82.
23. Feng QL, Wu J, Chen GQ, Cui FZ, Kim TN, Kim JO. A mechanistic study of the antibacterial effect of silver ions on *Escherichia coli* and *Staphylococcus aureus*. *J Biomed Mater Res*. 2000;52:662-8.
24. Raffi M, Hussain F, Bhatti TM, Akhter JI, Hameed A, Hasan MM. Antibacterial characterization of silver nanoparticles against *E. Coli* ATCC-15224. *J Mater Sci Technol*. 2008;24(2):192-6.
25. Alt V, Bechert T, Steinrücke P, Wagener M, Seidel P, Dingeldein E, et al. An in vitro assessment of the antibacterial properties and cytotoxicity of nanoparticulate silver bone cement. *Biomaterials*. 2004;25:4383-91.
26. Li Y-F, Chen C. Fate and toxicity of metallic and metal-containing nanoparticles for biomedical applications. *Small*. 2011;7:2965-80.
27. Chen W, Liu Y, Courtney HS, Bettenga M, Agrawal CM, Bumgardner JD, et al. In vitro anti-bacterial and biological properties of magnetron co-sputtered silver-containing hydroxyapatite coating. *Biomaterials*. 2006;27:5512-7.
28. Allan I, Newman H, Wilson M. Antibacterial activity of particulate Bioglass® against supra- and subgingival bacteria. *Biomaterials*. 2001;22:1683-7.
29. Zhang D, Leppäranta O, Munukka E, Ylänen H, Viljanen MK, Eerola E, et al. Antibacterial effects and dissolution behavior of six bioactive glasses. *J Biomed Mater Res A*. 2010;93:475-83.
30. Chen QZ, Thompson ID, Boccaccini AR. 45S5 Bioglass®-derived glass-ceramic scaffolds for bone tissue engineering. *Biomaterials*. 2006;27:2414-25.
31. Chen QZ, Thouas GA. Fabrication and characterization of sol-gel derived 45S5 Bioglass -ceramic scaffolds. *Acta Biomater*. 2011;7:3616-26.
32. Esteban-Tejeda L, Zheng K, Prado C, Cabal B, Torrecillas R, Boccaccini AR, et al. Bone tissue scaffolds based on antimicrobial SiO₂-Na₂O-Al₂O₃-CaO-B₂O₃ glass. *J Non-Cryst Solids*. 2016;432:73-80.
33. El-Sayed SAM, Mabrouk M, Khallaf ME, Abd El-Hady BM, El-Meliogy E, Shehata MR. Antibacterial, drug delivery, and osteoinduction abilities of bioglass/chitosan scaffolds for dental applications. *J Drug Deliv Sci Technol*. 2020;57:101757.
34. Spirandeli BR, Ribas RG, Amaral SS, Martins EF, Esposito E, Vasconcelos LMR, et al. Incorporation of 45S5 bioglass via sol-gel in β -TCP scaffolds: bioactivity and antimicrobial activity evaluation. *Mater Sci Eng C*. 2021;131:112453.
35. Ahmed AA, Ali AA, Mahmoud DAR, El-Fiqi AM. Preparation and characterization of antibacterial P2O₅-CaO-Na₂O-Ag₂O glasses. *J Biomed Mater Res A*. 2011;98A(1):132-42.
36. Hu S, Chang J, Liu M, Ning C. Study on antibacterial effect of 45S5 Bioglass®. *J Mater Sci Mater Med*. 2009;20:281-6.
37. Echezarreta-López MM, Landin M. Using machine learning for improving knowledge on antibacterial effect of bioactive glass. *Int J Pharm*. 2013;453:641-7.
38. Oliveira AP, Motisuke M, Leal Cv, Beppu MM. A comparative study between β -TCP prepared by solid state reaction and by aqueous solution precipitation: application in cements. *Key Eng Mater*. 2008;361-363(1):355-8.
39. Cardoso HAI, Motisuke M, Zavaglia CAC. Análise da influência de dois processos distintos de moagem nas propriedades do pó precursor e do cimento de beta-TCP. *Ceramica*. 2012;58:225-8.
40. Spirandeli BR, Campos TMB, Ribas RG, Thim GP, Trichês ES. Evaluation of colloidal and polymeric routes in sol-gel synthesis of a bioactive glass-ceramic derived from 45S5 bioglass. *Ceram Int*. 2020;46:20264-71.

41. Turkevich J, Stevenson PC, Hillier J. A study of the nucleation and growth processes in the synthesis of colloidal gold. *Discuss Faraday Soc.* 1951;11:55.
42. Gorup LF, Longo E, Leite ER, Camargo ER. Moderating effect of ammonia on particle growth and stability of quasi-monodisperse silver nanoparticles synthesized by the Turkevich method. *J Colloid Interface Sci.* 2011;360(2):355-8. <https://doi.org/10.1016/j.jcis.2011.04.099>.
43. Reid JW, Pietak A, Sayer M, Dunfield D, Smith TJN. Phase formation and evolution in the silicon substituted tricalcium phosphate/apatite system. *Biomaterials.* 2005;26:2887-97.
44. Duncan J, Hayakawa S, Osaka A, MacDonald JF, Hanna JV, Skakle JM, Gibson IR. Furthering the understanding of silicate-substitution in α -tricalcium phosphate: an X-ray diffraction, X-ray fluorescence and solid-state nuclear magnetic resonance study. *Acta Biomater.* 2014;10:1443-50.
45. Pietak AM, Reid JW, Stott MJ, Sayer M. Silicon substitution in the calcium phosphate bioceramics. *Biomaterials.* 2007;28:4023-32.
46. Santos SC, Barreto LS, dos Santos EA. Nanocrystalline apatite formation on bioactive glass in a sol-gel synthesis. *J Non-Cryst Solids.* 2016;439:30-7.
47. Hesaraki S, Safari M, Shokrgozar MA. Development of beta-tricalcium phosphate/sol-gel derived bioactive glass composites: physical, mechanical, and in vitro biological evaluations. *J Biomed Mater Res B Appl Biomater.* 2009;91:459-69.
48. Cacciotti I, Lombardi M, Bianco A, Ravaglioli A, Montanaro L. Sol-gel derived 45S5 bioglass: Synthesis, microstructural evolution and thermal behaviour. *J Mater Sci Mater Med.* 2012;23:1849-66.
49. Galván-Chacón VP, Eqtasadi S, Pajares A, Miranda P, Guiberteau F. Elucidating the role of 45S5 bioglass content in the density and flexural strength of robocast β -TCP/45S5 composites. *Ceram Int.* 2018;44:12717-22.
50. Bergmann C, Lindner M, Zhang W, Koczur K, Kirsten A, Telle R, et al. 3D printing of bone substitute implants using calcium phosphate and bioactive glasses. *J Eur Ceram Soc.* 2010;30:2563-7.
51. Carrodeguas RG, de Aza S. α -Tricalcium phosphate: Synthesis, properties and biomedical applications. *Acta Biomater.* 2011;7:3536-46.
52. Xin R, Leng Y, Chen J, Zhang Q. A comparative study of calcium phosphate formation on bioceramics in vitro and in vivo. *Biomaterials.* 2005;26:6477-86.
53. Juhasz JA, Best SM, Bonfield W, Kawashita M, Miyata N, Kokubo T, et al. Apatite-forming ability of glass-ceramic apatite-wollastonite - Polyethylene composites: effect of filler content. *J Mater Sci Mater Med.* 2003;14:489-95.
54. Sepulveda P, Ortega FS, Innocentini MDM, Pandolfelli VC. Properties of highly porous hydroxyapatite obtained by the gelcasting of foams. *J Am Ceram Soc.* 2000;83:3021-4.
55. Sepulveda P, Binner JGP. Processing of cellular ceramics by foaming and in situ polymerisation of organic monomers. *J Eur Ceram Soc.* 1999;19:2059-66.
56. Tripathi G, Ishikawa K. Fabrication and in vitro dissolution evaluation of low-crystalline β -TCP blocks through aqueous solution mediated phase conversion. *Mater Sci Eng C.* 2019;101:228-31.
57. Jilavenkatesa A, Condrate RA. The infrared and raman spectra of β - and α - tricalcium phosphate ($\text{Ca}_3(\text{PO}_4)_2$). *Spectrosc Lett.* 1998;31:1619-34.
58. Sayer M, Stratilatov AD, Reid J, Calderin L, Stott MJ, Yin X, et al. Structure and composition of silicon-stabilized tricalcium phosphate. *Biomaterials.* 2003;24:369-82.
59. Qiu ZY, Noh IS, Zhang SM. Silicate-doped hydroxyapatite and its promotive effect on bone mineralization. *Front Mater Sci.* 2013;7:40-50.
60. Birchall JD, Espie AW. Biological implications of the interaction (via silanol groups) of silicon with metal ions. *Ciba Found Symp.* 1986;121:140-59.
61. Birchall JD. The essentiality of silicon in biology. *Chem Soc Rev.* 1995;24:351.
62. Reffitt DM, Ogston N, Jugdaohsingh R, Cheung HF, Evans BA, Thompson RP, et al. Orthosilicic acid stimulates collagen type 1 synthesis and osteoblastic differentiation in human osteoblast-like cells in vitro. *Bone.* 2003;32:127-35.
63. de Bernardis F, Mühlshlegel FA, Cassone A, Fonzi WA. The pH of the host niche controls gene expression in and virulence of *Candida albicans*. *Infect Immun.* 1998;66:3317-25.
64. Nostro A, Cellini L, Di Giulio M, D'Arrigo M, Marino A, Blanco AR, et al. Effect of alkaline pH on staphylococcal biofilm formation. *APMIS.* 2012;120:733-42.